

Improved AutoEncoder with LSTM module and KL divergence for anomaly detection

Wei Huang, Bingyang Zhang, Kaituo Zhang, Hua Gao and Rongchun Wan

Abstract—The task of anomaly detection is to separate anomalous data from normal data in the dataset. Models such as deep convolutional autoencoder (CAE) network and deep supporting vector data description (SVDD) model have been universally employed and have demonstrated significant success in detecting anomalies. However, the over-reconstruction ability of CAE network for anomalous data can easily lead to high false negative rate in detecting anomalous data. On the other hand, the deep SVDD model has the drawback of feature collapse, which leads to a decrease of detection accuracy for anomalies. To address these problems, we propose the Improved AutoEncoder with LSTM module and Kullback-Leibler divergence (IAE-LSTM-KL) model in this paper. An LSTM network is added after the encoder to memorize feature representations of normal data. In the meanwhile, the phenomenon of feature collapse can also be mitigated by penalizing the featured input to SVDD module via KL divergence. The efficacy of the IAE-LSTM-KL model is validated through experiments on both synthetic and real-world datasets. Experimental results show that IAE-LSTM-KL model yields higher detection accuracy for anomalies. In addition, it is also found that the IAE-LSTM-KL model demonstrates enhanced robustness to contaminated outliers in the dataset.

Index Terms—LSTM, Deep SVDD, autoencoder, hypersphere collapse, anomaly detection.

I. INTRODUCTION

IN recent years, the topic of anomaly detection has emerged as a popular research topic in both science and application fields. The goal of anomaly detection is to distinguish a small fraction of unexpected samples from a large number of data samples. The applications of anomaly detection span across various domains, which include intrusion detection systems of networks [1], fraud detection systems [2] and so on. To address the task of anomaly detection, unsupervised learning methods have been widely employed in recent years. In contrast to supervised or semi-supervised learning, unsupervised

learning has the advantage of better suitability to situations where labeled or categorized information is scarce. In the context of anomaly detection, unsupervised learning can uncover potential patterns or abnormal behavior from unlabeled data without the need of an abundance of labeled samples [3, 4, 5]. Therefore, we mainly focus on unsupervised anomaly detection in this study.

To cope with the task of anomaly detection, the Convolutional AutoEncoder (CAE) [6] model, a classic type of neural network architecture, has gained significant attention for their ability to learn compressed, meaningful representations of high-dimensional data. The common assumption of CAE is that the reconstruction error tends to be lower for normal inputs, and is anticipated to increase for abnormal inputs. However, the CAE model has the drawback that this model can sometimes reconstruct anomalous inputs very well, thus resulting in lower reconstruction error for anomalous inputs. As a result, anomalous samples can hardly be distinguished from normal samples under the CAE model.

Due to the limited discriminative ability of CAE model for normal and abnormal inputs, researchers then proposed a few other variants of CAE such as Variational Autoencoder (VAE) [7] to enhance the power of autoencoder network in anomaly detection. The VAE model offers performance improvement over the CAE by generating smooth, continuous samples with a structured latent space, providing probabilistic modeling for uncertainty estimation, and facilitating meaningful interpolation in the latent space. In addition, to improve the discriminative capacity of CAE, [8] incorporated a memory module to confine the latent space of an autoencoder in the context of video anomaly detection. [9] introduced transformer structure to enhance the performance of the autoencoder network in anomaly detection on multivariate time-series data. Compared to the CAE model, the transformer-based method shows more computational efficiency while not compromising performances of anomaly detection.

Support Vector Data Description (SVDD) [10] represents another kind of unsupervised learning designed for one-class classification. The primary objective is to characterize the inherent structure of data samples by enveloping the majority of data points within a hypersphere

This work was supported by the National Key R&D Program of China (2022YFE0198900) and the National Natural Science Foundation of China (61771430).

Wei Huang, Bingyang Zhang, Kaituo Zhang and Hua Gao are with the College of Computer Science, Zhejiang University of Technology, Hangzhou, 310023, China.

Rongchun Wan is with Zhejiang HOUAR Intelligent Technology Co., Ltd., Hangzhou, 310023, China.

Hua Gao is the corresponding author (e-mail: ghua@zjut.edu.cn).

in the high dimensional space. Nevertheless, similar to many other machine-learning algorithms, SVDD also cannot work well in high-volume and high-dimensional dataset such as image or video dataset. This is mainly because SVDD is a kind of shallow method which cannot sufficiently capture intrinsic deep features in high-dimensional space. To address this problem, Deep Support Vector Data Description (Deep SVDD) [11], an unsupervised deep-learning approach for one-class classification, has been proposed recently. This approach is inspired by the shallow SVDD and reduces the data dimension into an appropriate size which is realized by an encoder module of an autoencoder, mapping the original high-dimensional data into feature vectors lying in the closed hypersphere space. However, [11] pointed out that Deep SVDD has the problem of hypersphere collapse, in which all data points are mapped to a single point in feature space, losing the ability to distinguish anomalous data from normal data. This problem can be partially overcome by removing bias terms of all hidden layers since the network with the bias term in any hidden layer can be trained into a constant function mapping all data into the hypersphere center, leading to hypersphere collapse [11].

In addition, based on Deep SVDD, [12] proposed the Multilayer One-Class Classification (MOCCA) [12] which incorporates the output of each layer into the loss function. MOCCA employs a strategy akin to skip connections in backpropagation, aiming at reducing the number of effective layer and ensuring comprehensive training for the initial layers of the network. [13] extended Deep SVDD to a patch-based approach (called Patch SVDD) [13] by incorporating self-supervised learning, aiming at preserving original information and reducing dimensionality. However, this extension encounters the challenge of insufficient sampling, and the overall algorithm may not be entirely rational. Since the Patch SVDD model serves the sole purpose of downscaling images, ultimately, a nearest-neighbor algorithm is employed for binary classification. Therefore, the Patch SVDD model is constrained by the bottleneck in handling with high-dimensional data that is usually encountered in traditional machine-learning algorithms.

Although these methods have shown some improvements over CAE or Deep SVDD models, there is still significant room for further enhancing the performance of anomaly detection since these methods are still unable to effectively distinguish abnormal samples from normal samples. One possible reason is that these models have not sufficiently utilized feature vectors in the hidden space to perform the task of anomaly detection. For example, the over-reconstruction ability of autoencoder network can result in more false negatives in detecting anomalies, since these autoencoder-based models do not

impose additional effective constraints on the feature vectors in the hidden space. In addition, in Deep SVDD related works, the phenomenon of features collapse in the hidden space can easily occur, which can also hinder the distinction of anomalous data from normal data.

To address the above-mentioned problems, we propose the Improved AutoEncoder with LSTM module and KL divergence (called IAE-LSTM-KL for short) approach in this paper. We explore the potential of CAE network combined with the Deep SVDD to extract intrinsic data features and generate accurate reconstructions. Considering that the LSTM module excels in capturing temporal features of time-series data, we add an LSTM layer between the encoder and the decoder to store feature representations learned in the training stage. The LSTM layer has the role of memorizing feature representations from normal samples. By treating the input data in the training stage as a temporal sequence, the LSTM layer can inherently retain information in the initial stage, or receive the encoding from the output of CAE network. Moreover, the input gate and the output gate in LSTM module further filter out the impact of abnormal information by discerning the flow of information, ensuring the purity of normal data. In addition, to mitigate the phenomenon of feature collapse in Deep SVDD, we use the Kullback-Leibler (KL) divergence to force the feature vectors fed into the SVDD module following Gaussian distribution. By using KL divergence, the feature vectors fed into the SVDD module is shifted from the center of hypersphere towards outer periphery of hypersphere in the hidden space, thus reducing the possibility of feature collapse in Deep SVDD module. Experimental results demonstrate that the proposed IAE-LSTM-KL model exhibits faster convergence, higher stability and superior anomaly-detection performance as compared to other state-of-art methods. In addition, ablation experiments show that both LSTM layer and KL divergence penalty have positive impacts on the performance of IAE-LSTM-KL model in the task of anomaly detection.

The main contributions of this study are summarized as follows:

- We introduce a novel anomaly-detection model, called Improved AutoEncoder with LSTM module and KL divergence (IAE-LSTM-KL) in this paper, to simultaneously address the problem of over-reconstruction for anomalous data in CAE model and the problem of feature collapse in Deep SVDD model. This model is the combination of the autoencoder framework, the SVDD module, the LSTM module and the KL divergence penalty. Different from the one-class Deep SVDD and CAE models, the IAE-LSTM-KL model can preserve essential normal features while concurrently sieving out anomalous data, thus diminishing the total loss

relevant to normal cases.

- Extensive experiments have been carried out on multiple datasets, including both synthetic and real-world datasets. Results show that the proposed IAE-LSTM-KL model exhibits superior accuracy and reduced error rates as compared to other state-of-art anomaly-detection models.
- Experimental results also show that the IAE-LSTM-KL model demonstrates enhanced robustness to contaminated noises in the dataset. Even though the training set is contaminated with some outliers, the IAE-LSTM-KL model can still retain high capacity to detect anomalies, thereby endorsing the consistent enhanced robustness to noises in the dataset.

The rest of this paper is organized as follows. In Section II, we describe some preliminary work before formally introducing our proposed IAE-LSTM-KL model. In Section III, we describe the proposed IAE-LSTM-KL model in detail. In Section IV, the performances of the IAE-LSTM-KL model and several competing models in anomaly detection are compared through experiments on some datasets. Extensive discussions for experimental results are also presented in this section. Finally, some conclusions are drawn in Section V.

II. RELATED WORK

Before presenting our proposed model, in this section, we describe several prior works that are relevant to our work.

A. Convolutional AE (CAE)

The convolutional autoencoder (CAE) is a kind of unsupervised reconstruction-based neural network, which consists of an encoder $f_e(\cdot; \theta_e)$ and a decoder $f_d(\cdot; \theta_d)$. The CAE with multiple hidden layers can effectively capture intricate data hierarchies and dependencies. The encoder compresses input data into the lower-dimensional latent feature, while the decoder attempts to reconstruct the original data from the compressed representation. With the assumption that the CAE model is usually trained on normal data, the training objective is that abnormal inputs result in a larger reconstruction error than normal inputs in the testing phase. Specifically speaking, the dependency between the input data \mathbf{x} and the reconstructed signal $\hat{\mathbf{x}}$ can be expressed in the following equation:

$$\hat{\mathbf{x}} = f_d(f_e(\mathbf{x}; \theta_e); \theta_d). \quad (1)$$

In addition, the target loss function of the CAE model is to minimize

$$L = \min_{\theta_e, \theta_d} \|\mathbf{x} - \hat{\mathbf{x}}\|, \quad (2)$$

where $\|\cdot\|$ denotes the empirically measured l_1 -norm or l_2 -norm of the argument vector.

B. Deep SVDD

The Deep SVDD [11] model is a kind of one-class anomaly detection method which utilizes the encoder part of autoencoder. The training objective of Deep SVDD is to map normal samples into a constructed hypersphere with a center in the high-dimensional space. In the testing phase, normal samples fall within the hypersphere, while anomalous samples fall outside the hypersphere.

Now, we present the details of Deep SVDD model in the following. Define the input space $\mathcal{X} \subseteq R^d$ and hidden feature space \mathcal{F} . Given the input data $\mathbf{x} \in \mathcal{X}$, the expression $f_e(\cdot; \theta_e) : \mathbf{x} \rightarrow \mathbf{z}$ denote an encoder network with L hidden layers such as convolutional neural layer for image dataset, and a set of weights $\mathcal{W} = \{\mathbf{W}^1, \dots, \mathbf{W}^L\}$. Here, $\mathbf{z} \in \mathcal{F}$ denotes the feature representations of $\mathbf{x} \in \mathcal{X}$ in the hidden space. The aim of Deep SVDD is to jointly learn the network parameters \mathcal{W} together with minimizing the volume of a data-enclosing hypersphere in the feature space \mathcal{F} . The hypersphere is characterized by radius $R > 0$ and center $\mathbf{c} \in \mathcal{F}$. Given the training set $D_n = \{\mathbf{x}_1, \dots, \mathbf{x}_n\}$ on \mathcal{X} , [11] defines two different kinds of objective functions. The first is the soft-boundary Deep SVDD:

$$L_{soft} = \min_{\theta_e, R, \mathbf{W}} R^2 + \frac{1}{vn} \sum_{i=1}^n \max(0, \|\mathbf{z}_i - \mathbf{c}\|^2 - R^2) + \frac{\lambda}{2} \sum_{l=1}^L \|\mathbf{W}^l\|_F^2, \quad (3)$$

and the second is the hard-boundary Deep SVDD:

$$L_{hard} = \min_{\theta_e, \mathbf{W}} \frac{1}{n} \sum_{i=1}^n \|\mathbf{z}_i - \mathbf{c}\|^2 + \frac{\lambda}{2} \sum_{l=1}^L \|\mathbf{W}^l\|_F^2. \quad (4)$$

The last terms of both (3) and (4) are the weight decay regularizers to alleviate overfitting for the input data with the hyperparameter $\lambda > 0$. In addition, the hyperparameter v in (3) controls the degree of some points being mapped out of the hypersphere. The hard-boundary objective function (4) can be regarded as the simplified version of soft-boundary objection function when the most training data is normal. In our study, we shall apply both soft-boundary and hard-boundary versions in our proposed IAE-LSTM-KL model.

C. Improved AutoEncoder for Anomaly Detection (IAEAD)

As we have stated above, both CAE and Deep SVDD models have the capability of detecting anomalies. However, in the case that the training data is contaminated by some anomalous data, the CAE model can well reconstruct both normal and anomalous data, which leads

to high false negatives in anomaly detection. On the other hand, the Deep SVDD model has the drawback of easily suffering from feature collapse for anomaly detection, which mixes hidden features of both normal and abnormal samples together and results in indistinguishability of anomalous samples from normal samples.

To overcome the drawbacks of CAE and Deep SVDD models, [14] proposed an improved autoencoder model (called IAEAD) that combines the CAE with the Deep SVDD model. This improved model can efficiently implement the task of anomaly detection while learning representative features to preserve the local structure of input data. Specifically speaking, the IAEAD model is optimized by minimizing the following objective function:

$$L = \min_{\mathcal{W}} \alpha L_{rec} + L_{soft}, \quad (5)$$

As we can observe from (5), the objective function of IAEAD model is actually the weighted sum of L_{rec} and L_{soft} controlled by the hyperparameter α . Finally, we have to mention that the term L_{soft} can also be replaced by L_{hard} , forming the IAEAD model with hard-boundary Deep SVDD model.

III. PROPOSED METHOD

A. Framework of IAE-LSTM-KL model

The framework of IAE-LSTM-KL model is illustrated in Fig. 1. This model consists of three modules, i.e. the CAE module, the SVDD module and the LSTM module. The encoder in CAE module initially processes the input data to generate the latent feature vector in the feature space. Subsequently, the LSTM module utilizes this latent vector to capture the feature relationships between the input data and the stored normal data representatives. Then, the decoder in CAE module reconstructs the latent features generated from the LSTM module. Simultaneously, the role of SVDD module is to create a minimal hypersphere enclosing most latent features generated from the LSTM module.

As we have mentioned in the section of Introduction, the Deep SVDD model [11] has the drawback of feature collapse in the training process. Hypersphere collapse refers to the situation in which the model learns representations in the latent space that is too concentrated around a central point. Consequently, hypersphere collapse hinders the model to distinguish abnormal data samples from normal samples, leading to difficulties in detecting anomalies. To mitigate the phenomenon of feature collapse in Deep SVDD module, we use Kullback-Leibler (KL) divergence to force the latent features after the LSTM module following Gaussian distribution, which can provide more flexibility for latent features after the LSTM module to cover broader range of latent representation space. By using KL divergence to

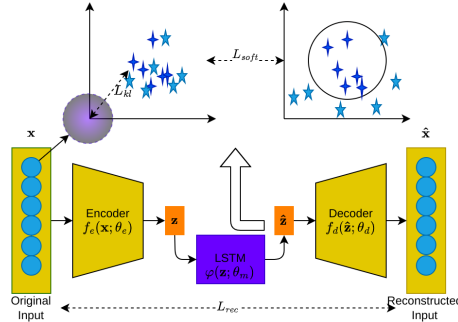


Fig. 1: Schematic representation of the IAE-LSTM-KL model. Compared to the IAEAD model [14], the IAE-LSTM-KL model add an LSTM layer between the encoder and the decoder. In addition, when training the hidden features under the SVDD model, the hidden features are also forced to follow standard Gaussian distribution using KL divergence penalty.

regulate the distribution of latent features, the proposed model can well preserve the diversity of latent features fed into the Deep SVDD module. Consequently, the robustness of the proposed IAE-LSTM-KL model in detecting anomalies can be enhanced.

In the training phase, the IAE-LSTM-KL model is assumed to be exclusively trained using normal data. The LSTM module continuously updates the contents stored in it, and memorizes the prototype representations of normal data. In the testing phase, even when an abnormal input is sent into the IAE-LSTM-KL model, the reconstructed data still resembles normal samples resulting in high reconstruction error since the reconstructed data is decoded from normal patterns in LSTM. As a result, the reconstruction error is still nontrivial if the input data is abnormal. In the meanwhile, the reconstruction error still remains to be low for normal input. Therefore, the LSTM module in the IAE-LSTM-KL model plays an important role in distinguishing anomalous data from normal inputs.

In the following part, we will firstly analyze the working mechanism of LSTM module. Then, we shall give the overview of the whole IAE-LSTM-KL in detail.

B. Introduction for LSTM module

The Long Short-Term Memory (LSTM)[15] is a type of memory that extracts similar information from the input data and stores them in it. Usually, a LSTM network consists of multiple cell units and the structure of each cell unit is demonstrated in Fig. 2(a). In the LSTM structure, c_t represents the cell state, which is used as the memory unit storing information from the previous cell unit and receiving information from current cell unit. In each cell unit, there are three gates, namely the input gate

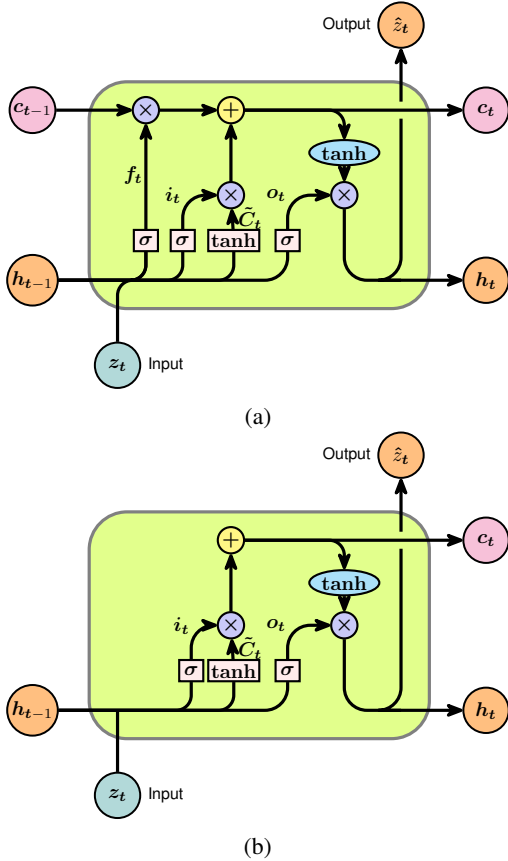


Fig. 2: (a). Demonstration of cell unit that is used in the original LSTM network. (b). Demonstration of degenerated cell unit that is used in our study.

i , the output gate o and the forget gate f respectively. The input gate controls the flow of information into the cell state c_t which contains the stored representatives of normal data. The role of input gate is to determine what to remember from the current input. The output gate decides what to output as the new hidden state using the sigmoid function. Finally, the forget gate regulates what to forget from the previous cell state.

Given the latent feature z_t which is the output of encoder, we have to decide what new information we are going to store in the cell state and establish the relationship between z_t and the stored cell state c_t . First, the input gate and the output gate respectively control the flow of information received by z_t and the flow of information output from c_t , which can be expressed as

$$\mathbf{i}_t = \sigma(\mathbf{W}_i \cdot [\mathbf{h}_{t-1}, \mathbf{z}_t] + \mathbf{b}_i) \quad (6)$$

and

$$\mathbf{o}_t = \sigma(\mathbf{W}_o \cdot [\mathbf{h}_{t-1}, \mathbf{z}_t] + \mathbf{b}_o) \quad (7)$$

respectively. Here, through dual control of input and output, we further refine the information flow to ensure

the purity of the regular information stream, thus filtering out anomalous data. In addition, the forget gate f_t is determined by both the \mathbf{h}_{t-1} and \mathbf{z}_t , which is expressed as

$$\mathbf{f}_t = \sigma(\mathbf{W}_f \cdot [\mathbf{h}_{t-1}, \mathbf{z}_t] + \mathbf{b}_f). \quad (8)$$

Next, a \tanh function creates a vector of new candidate values \tilde{C}_t , which is expressed as

$$\tilde{C}_t = \tanh(\mathbf{W}_C \cdot [\mathbf{h}_{t-1}, \mathbf{z}_t] + \mathbf{b}_C). \quad (9)$$

Then, the current cell state c_t is calculated based on the input gate \mathbf{i}_t , the forget gate \mathbf{f}_t , the previous cell state c_{t-1} , and the value \tilde{C}_t , which is shown as

$$\mathbf{c}_t = \mathbf{f}_t \odot \mathbf{c}_{t-1} + \mathbf{i}_t \odot \tilde{C}_t. \quad (10)$$

After passing through the output gate, the output \hat{z}_t , as well as \mathbf{h}_t , is finally obtained as

$$\hat{\mathbf{z}}_t = \mathbf{h}_t = \mathbf{o}_t \odot \tanh(\mathbf{c}_t), \quad (11)$$

where \odot denotes the operation of element-wise multiplication between two vectors with the same size.

In our study, we only utilize a single cell unit to form the LSTM structure, which indicates that we do not utilize the recurrent structure originally from LSTM structure. The latent representation z_t in our study is regarded as time-series data with only one time step. Therefore, both \mathbf{h}_{t-1} and \mathbf{c}_{t-1} are set to the fixed values \mathbf{h}_0 and \mathbf{c}_0 respectively. In our study, both \mathbf{h}_0 and \mathbf{c}_0 are set to zero matrices. In the case of $\mathbf{c}_0 = \mathbf{O}$, (10) becomes

$$\mathbf{c}_t = \mathbf{i}_t \odot \tilde{C}_t. \quad (12)$$

Fig. 2(b) demonstrates the degenerated LSTM cell unit that is used in our study. The main role of degenerated LSTM module can be described as follows. Firstly, by treating the training data as a temporal sequence, the data \tilde{C}_t inherently retains information from the initial stage or receive z_t from the encoder in CAE. Therefore, since the data in the training set are assumed to be normal, the cell unit preserves the prototypical normal patterns in the normal set and stores them into \tilde{C}_t . Secondly, in the testing phase, the input gate has the role of filtering out the input z_t to the cell unit. Therefore, the input gate can remove abnormal information while retaining the information of normal samples. Furthermore, the output gate can further filter out abnormal information to distinguish anomalous data from normal data in more effective way.

Through the above analysis, it is evident that the LSTM module is capable of memorizing normal patterns in the training set. Actually, we have also noticed that the memory module in the MemAE model [8] also has the function of memorization. However, due to the possible presence of abnormal data in the training set, the memory module in [8] records normal patterns in

the memory unit containing a set of vectors. The weight assigned to each vector in the memory unit for choosing the pattern that well matches the input data needs to be calculated. However, the memory module in [8] has the drawback that any interference in the weights would bias the latent representation from the memory module, which subsequently affects the distinguishing ability of autoencoder structure. In contrast, in the LSTM module, both input gate and output gate can filter out the input information flow, due to which the interference of abnormal information flow can be mitigated. Furthermore, the cell unit in LSTM neither saves multiple state vectors nor uses weighted summing, thereby enhancing the purity of the normal information flow.

C. Detailed introduction for the IAE-LSTM-KL model

In this section, we shall describe our proposed IAE-LSTM-KL model in detail. Fig. 1 demonstrates the whole structure of IAE-LSTM-KL model. Considering the batch of input data $\{\mathbf{x}_1, \mathbf{x}_2, \dots, \mathbf{x}_n\} \in \mathcal{X}$, where n denotes the total number of input samples, the objective of the IAE-LSTM-KL model is to distinguish abnormal samples from normal samples in more efficient way by means of LSTM to better separate abnormal samples from normal samples, and KL divergence to avoid feature collapse in SVDD training.

Define $\varphi(\cdot; \theta_m) : \mathbf{z} \rightarrow \hat{\mathbf{z}}$ as the process of LSTM module, where $\hat{\mathbf{z}}$ is the output vector (in the hidden feature space) of LSTM module. The data $\hat{\mathbf{z}}$ are then fed into two other modules, which are the SVDD module and the decoder module respectively. The role the SVDD module is to enforce normal samples getting closer by constructing a hypersphere with the minimal volume enclosing features vectors of all normal samples. At the same time, the data $\hat{\mathbf{z}}$ in the hidden space are decoded to generate the reconstructed data via the mapping $f_d(\cdot; \theta_d) : \hat{\mathbf{z}} \rightarrow \hat{\mathbf{x}}$, where $\hat{\mathbf{x}}$ is the output of decoder as the reconstructed data of \mathbf{x} . In addition, we have to mention that in the training process, the data $\hat{\mathbf{z}}$ are enforced following the standard Gaussian distribution by using the penalty of KL divergence. The use of KL divergence can be helpful for broadening the distribution of output data from LSTM module to mitigate the chance of feature collapse in the SVDD module.

In our work, we optimize the IAE-LSTM-KL model by minimizing the total loss L_{total} which includes the Deep SVDD loss L_{svdd} , the KL divergence L_{kl} between $\hat{\mathbf{z}}$ and standard Gaussian distribution, and the reconstruction loss L_{rec} from the CAE model. The objective function of the IAE-LSTM-KL model can be expressed as the following weighted sum of L_{svdd} , L_{kl} and L_{rec} :

$$L_{total} = L_{svdd} + \lambda_1 L_{kl} + \lambda_2 L_{rec}, \quad (13)$$

where the hyperparameters λ_1 and λ_2 are used to trade off different kinds of losses. For the SVDD loss L_{svdd} , we can use either the soft-boundary version L_{soft} or the hard-boundary version L_{hard} .

In addition, the reconstruction loss from the CAE module is defined as

$$L_{rec} = \frac{1}{n} \sum_{i=1}^n \|\mathbf{x}_i - \hat{\mathbf{x}}_i\|^2. \quad (14)$$

With L_{svdd} , L_{kl} and L_{rec} , the total loss of the IAE-LSTM-KL model with soft-version of SVDD can be expressed as:

$$\begin{aligned} \min_{\theta_e, \theta_d, R, \mathcal{W}} R^2 + \frac{1}{vn} \sum_{i=1}^n \max(0, \|\hat{\mathbf{z}}_i - \mathbf{c}\|^2 - R^2) \\ + \frac{\lambda_1}{n} \sum_{i=1}^n KL(\hat{\mathbf{z}}_i \| \mathcal{N}_{\mathbf{0}, \mathbf{I}}) + \frac{\lambda_2}{n} \sum_{i=1}^n \|\mathbf{x}_i - \hat{\mathbf{x}}_i\|^2 \\ + \frac{\lambda_3}{2} \sum_{l=1}^L \|\mathbf{W}^l\|_F^2. \end{aligned} \quad (15)$$

When the soft-boundary of SVDD is replaced by hard-boundary SVDD, the total loss becomes

$$\begin{aligned} \min_{\theta_e, \theta_d, \mathcal{W}} \frac{1}{n} \sum_{i=1}^n \|\hat{\mathbf{z}}_i - \mathbf{c}\|^2 + \frac{\lambda_1}{n} \sum_{i=1}^n KL(\hat{\mathbf{z}}_i \| \mathcal{N}_{\mathbf{0}, \mathbf{I}}) \\ + \frac{\lambda_2}{n} \sum_{i=1}^n \|\mathbf{x}_i - \hat{\mathbf{x}}_i\|^2 + \frac{\lambda_3}{2} \sum_{l=1}^L \|\mathbf{W}^l\|_F^2. \end{aligned} \quad (16)$$

The last term in the above two objection functions is the decay regularizer on the network weight \mathcal{W} which denotes a network with L hidden layers such as convolutional neural layer for image dataset, and a set of weights $\mathcal{W} = \{\mathbf{W}^1, \dots, \mathbf{W}^L\}$ with the hyperparameter $\lambda_3 > 0$.

In the testing stage, we resolve to detect anomalies by measuring the distance between the feature vector of testing sample to the hypersphere center in the hidden feature space, which is defined as

$$SCORE = \|\hat{\mathbf{z}} - \mathbf{c}\|^2. \quad (17)$$

IV. EXPERIMENTS

In this section, we shall evaluate the performance of our proposed IAE-LSTM-KL model by comparing it with several other state-of-art models in the experiments for anomaly detection. Our experiments are carried out on three image datasets and one time-series dataset. Below we shall firstly describe the datasets that are used in our experiments. Then, we shall present and analyze experimental results of the proposed IAE-LSTM-KL model and several other competing models.

A. Datasets

In our study, we have carried out extensive experiments on three commonly-used image datasets, which are CIFAR10 [16], Fashion MNIST [17] and MVTec AD [18] datasets, and one time-series dataset, i.e. the Wind Turbine Blade Icing (WTBI) dataset. Both CIFAR10 and Fashion MNIST datasets have multiple classes and are originally used for classification. To reduce luminance difference between dark and light pixels in the image, we perform global contrast normalization using l_1 -norm for the images in both CIFAR10 and Fashion MNIST datasets before the training stage. In the experiments on these two image datasets, we designate one class as normal and the others as abnormal. The MVTec AD dataset is a comprehensive collection of defect-free and defective images of various object types and materials, designed to facilitate the development and evaluation of anomaly-detection algorithms in the scenario of industrial inspection. In addition, the WTBI dataset is collected from the measurements of wind turbines. To apply our proposed and other state-of-art competing methods to the WTBI dataset, we transform the time-series data into the image-like data to detect abnormal events that are hidden in the time-series data. Below are the brief introductions for the above datasets.

1). *CIFAR10*: The CIFAR10 dataset consists of 60,000 32×32 RGB color images categorized into 10 different classes [16]. The training and testing set consist of 50,000 and 10,000 samples respectively.

2). *Fashion MNIST*: The Fashion MNIST dataset was created in 2017 and consists of 70,000 grayscale images with 28×28 pixels forming 10 classes [17]. This dataset is divided into two parts with 60,000 images in the training set and 10,000 images in the testing set.

3). *WTBI*: The WTBI dataset was collected from the SCADA (Supervisory Control and Data Acquisition) system of wind turbine units. This dataset consists of SCADA information from multiple turbines within a wind farm, collected over a duration of two months. In this dataset, there are totally over a million timestamps of SCADA monitoring data. Each timestamp vector includes 28 continuous-value monitoring variables, covering various dimensions such as operational parameters, environmental conditions, and status parameters of turbines. The data in WTBI dataset are divided into two categories, i.e. non-icing period and icing period, with the non-icing and icing periods identified as normal and abnormal states respectively. Since the CAE structure is involved in both our proposed IAE-LSTM-KL and other competing state-of-art models, the WTBI dataset is firstly converted into image-like format for further training in anomaly-detection models before training. The data was firstly preprocessed by taking the average of previous and next five timestamps in order to smooth

data between adjacent time periods. Then, adjacent data was concatenated into a 26×26 matrix which was subsequently converted into a tensor vector. Using the sliding step of one unit, we finally obtained 39,438 normal and 2,814 abnormal image-like samples. The testing set was formed by combing 30% of normal and all abnormal image-like samples. Finally, we have 27,606 training samples and 14,646 testing samples.

4). *MVTec AD*: This dataset contains a carefully curated collection of images spanning a wide range of materials and products commonly found in industrial manufacturing settings [18], which contains more than 5,000 high-resolution images meticulously categorized into fifteen distinct classes. Each class includes a specified kind of objects and textures. Within each category, there are pristine training images, a selection demonstrating various defects, and additional defect-free images. Each image in this dataset is sized with 300×300 pixels, making it a comprehensive resource for conducting research in anomaly detection.

B. Results

The Area Under the Receiver Operating Characteristic (AUROC) evaluation has been widely adopted in numerous existing studies as the benchmark for assessing classification performance in terms of discrimination accuracy [19, 20, 21]. This evaluation facilitates straightforward comparisons across different models, as it does not necessitate the selection of classification thresholds or any additional parameters during calculation. In addition, to demonstrate the effectiveness of the proposed IAE-LSTM-KL model, we have conducted comprehensive comparisons between IAE-LSTM-KL and several other state-of-the-art models including CAE [6], MemAE [8], LSA [22], Deep SVDD [11] and IAEAD [14].

We utilize the notation $\text{Conv2}(s_{in}, s_{out}, k)$ and $\text{DConv2}(s_{int}, s_{out}, k)$ to denote the two-dimensional convolutional and deconvolutional layers respectively, with s_{in} , s_{out} , and k representing input channel size, output channel size, and kernel size respectively. In addition, a Linear layer is denoted by $\text{Linear}(n_{in}, n_{out})$, where n_{in} and n_{out} represent the number of input and output features respectively. Similarly, we use the notation $\text{LSTM}(n_{in}, n_{out})$ to represent the LSTM layer, with n_{in} and n_{out} represent the number of input and output features respectively.

For the CIFAR10, Fashion MNIST and WTBI datasets, we use three convolutional layers to implement the encoder: $\text{Conv2}(c, 32, 5)$ - $\text{Conv2}(32, 64, 5)$ - $\text{Conv2}(64, 128, 5)$, where c indicates the number of image channels. The decoder is implemented as $\text{Dconv2}(8, 128, 5)$ - $\text{Dconv2}(128, 64, 5)$ - $\text{Dconv2}(64, 32, 5)$ - $\text{Dconv2}(32, c, 5)$. Since only the CIFAR10 dataset contains the colored images, we set $c = 3$ for the CIFAR10

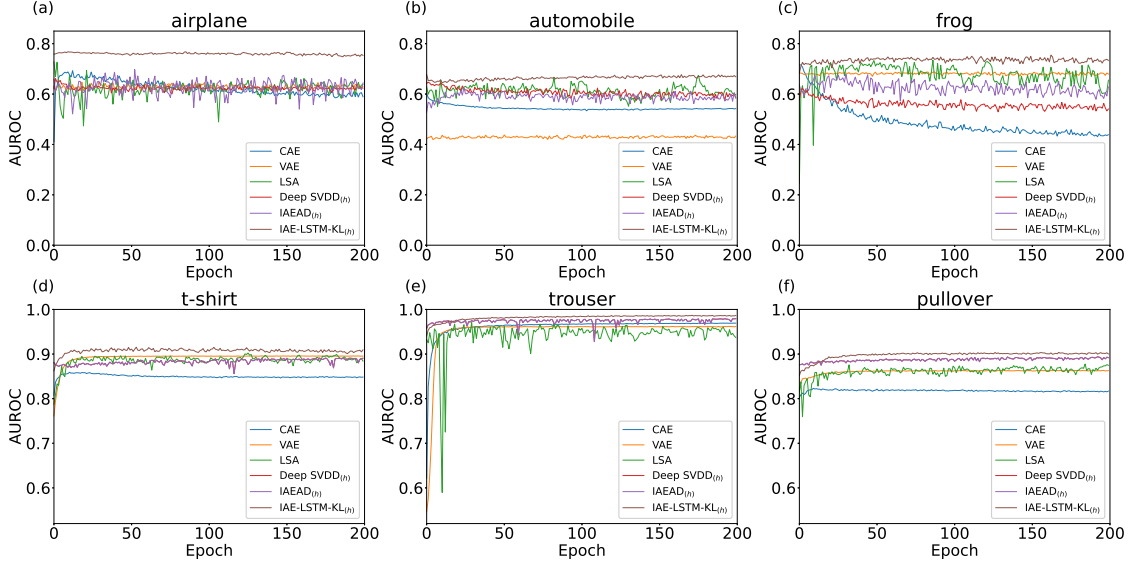


Fig. 3: AUROC values *versus* epochs in the training stage in CIFAR10 and Fashion MNIST datasets. The normal class in the dataset is shown above each subfigure. The training set only contains normal samples. For CIFAR10, the airplane, automobile and frog classes are chosen as normal data in (a), (b) and (c) respectively. For Fashion MNIST, the t-shirt, trouser and pullover classes are chosen as normal data in (d), (e) and (f) respectively.

TABLE I: AUROC for the CIFAR10 dataset. The subscripts (*s*) and (*h*) refer to the soft-boundary and hard-boundary SVDD, respectively. We highlight in bold the performance of the top-performing models.

Class	airplane	automobile	bird	cat	deer	dog	frog	horse	ship	truck	Avg.
CAE	0.581	0.531	0.488	0.571	0.497	0.601	0.441	0.557	0.739	0.612	0.562
MemAE	0.658	0.537	0.483	0.593	0.497	0.621	0.442	0.570	0.789	0.624	0.581
VAE	0.629	0.433	0.618	0.499	0.730	0.516	0.679	0.522	0.668	0.539	0.583
LSA	0.621	0.602	0.480	0.561	0.606	0.609	0.658	0.632	0.780	0.723	0.627
Deep SVDD(<i>h</i>)	0.621	0.620	0.486	0.576	0.569	0.633	0.578	0.614	0.777	0.688	0.616
Deep SVDD(<i>s</i>)	0.616	0.620	0.481	0.563	0.563	0.614	0.588	0.617	0.772	0.681	0.611
IAEAD(<i>h</i>)	0.637	0.590	0.500	0.557	0.597	0.581	0.637	0.631	0.725	0.663	0.612
IAEAD(<i>s</i>)	0.632	0.583	0.506	0.590	0.543	0.613	0.582	0.632	0.768	0.670	0.612
IAE-LSTM-KL(<i>h</i>)	0.780	0.688	0.613	0.648	0.706	0.650	0.759	0.658	0.798	0.777	0.708
IAE-LSTM-KL(<i>s</i>)	0.761	0.642	0.611	0.670	0.703	0.695	0.725	0.643	0.752	0.735	0.694

TABLE II: AUROC for the Fashion MNIST dataset. The subscripts (*s*) and (*h*) refer to the soft-boundary and hard-boundary SVDD, respectively. We highlight in bold the performance of the top-performing models.

Class	t-shirt	trouser	pullover	dress	coat	sandal	shirt	sneaker	bag	ankle-boot	Avg.
CAE	0.846	0.966	0.813	0.855	0.890	0.571	0.728	0.942	0.838	0.984	0.843
MemAE	0.901	0.987	0.885	0.916	0.883	0.898	0.782	0.988	0.861	0.980	0.908
VAE	0.896	0.962	0.863	0.884	0.894	0.347	0.773	0.968	0.853	0.983	0.842
LSA	0.886	0.940	0.862	0.867	0.895	0.474	0.766	0.941	0.916	0.984	0.853
Deep SVDD(<i>h</i>)	0.860	0.980	0.836	0.872	0.892	0.684	0.758	0.948	0.934	0.973	0.874
Deep SVDD(<i>s</i>)	0.863	0.977	0.851	0.882	0.891	0.649	0.775	0.951	0.923	0.975	0.874
IAEAD(<i>h</i>)	0.878	0.941	0.871	0.853	0.907	0.543	0.781	0.955	0.891	0.986	0.861
IAEAD(<i>s</i>)	0.864	0.961	0.851	0.856	0.895	0.692	0.759	0.953	0.879	0.986	0.870
IAE-LSTM-KL(<i>h</i>)	0.915	0.987	0.905	0.945	0.928	0.874	0.814	0.990	0.955	0.992	0.931
IAE-LSTM-KL(<i>s</i>)	0.887	0.981	0.891	0.915	0.912	0.923	0.815	0.973	0.944	0.981	0.922

dataset. For the remaining two datasets, i.e. Fashion MNIST and WTBI datasets, we set $c = 1$. Besides,

each layer of the autoencoder is followed by batch normalization (BN) [23] and a leaky ReLU activation

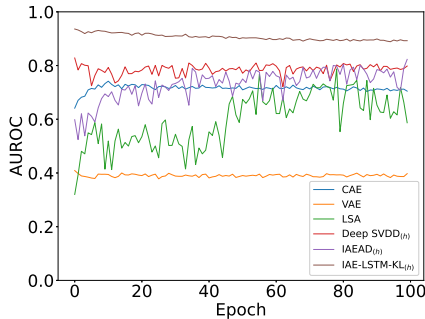


Fig. 4: AUROC values *versus* epochs in the training stage on the WTBI dataset.

TABLE III: AUROC for the WTBI dataset. The subscripts (*s*) and (*h*) refer to the soft-boundary and hard-boundary SVDD, respectively. We emphasize in bold the performance of the best models.

Models	AUROC
CAE	0.704
MemAE	0.690
VAE	0.392
LSA	0.685
Deep SVDD(<i>h</i>)	0.798
Deep SVDD(<i>s</i>)	0.823
IAEAD(<i>h</i>)	0.823
IAEAD(<i>s</i>)	0.894
IAE-LSTM-KL(<i>h</i>)	0.893
IAE-LSTM-KL(<i>s</i>)	0.963

[24], except for the last Dconv2 layer which is appended by a sigmoid function. Additionally, a max pooling layer is included following each activation function in the encoder, with both kernel size and stride set to 2. For the LSTM module, we use two layers, i.e. LSTM(2048, 2048)-Linear(2048, 128), to implement the LSTM module. Referring to the MVTec AD dataset, we use encoder and decoder with higher capacities. For the encoder, we use Conv2(3,96,3)-Conv2(96,128,3)-Conv2(128,256,3)-Conv2(256,256,3), while for the decoder, we use Dconv2(256,256,3)-Dconv2(256,128,3)-Dconv2(128,96,3)-Dconv2(96,3,3). Each layer is also followed by batch normalization (BN) and a leaky ReLU activation, except for the last Dconv2 layer. Finally, the LSTM module is implemented as LSTM(4096, 4096).

Comparing results for all competing models on CIFAR10, Fashion MNIST, WTBI and MVTec AD datasets which are demonstrated in Table I, Table II, Table III and Table IV respectively, it can be observed from these results that the proposed IAE-LSTM-KL model exhibits higher average AUROC values than other state-of-art models. Moreover, we have also observed that in the IAE-LSTM-KL model, the performances of anomaly detection are basically in the same level when using

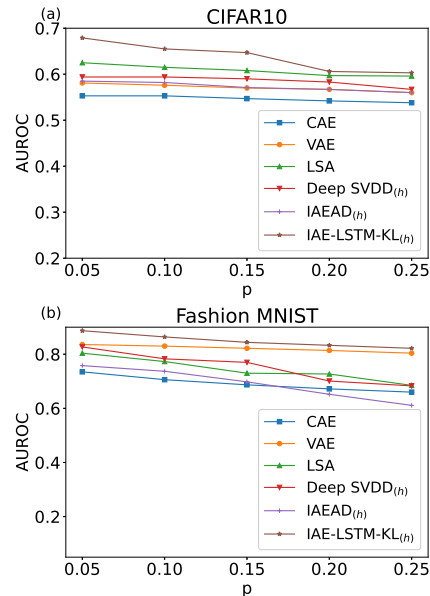


Fig. 5: Relationship between AUROC values and anomaly ratio on the training set. (a). CIFAR10 dataset. (b). Fashion MNIST dataset.

soft-boundary SVDD module and hard-boundary SVDD module respectively. These results show that our proposed IAE-LSTM-KL model is superior to the competing models in anomaly detection.

Fig. 3 and Fig. 4 demonstrate the change of AUROC values of all models in the training stage on CIFAR10, Fashion MNIST and WTBI datasets. It can be observed that AUROC values of the IAE-LSTM-KL model consistently reach high levels from the outset of training process thanks to the pretraining operation before the formal training for the IAE-LSTM-KL model. In addition, we have also found that AUROC values of the IAE-LSTM-KL model stabilize at the highest level among all models under study from the initial stage of training process. Moreover, AUROC values of the IAE-LSTM-KL model fluctuate only slightly in the steady-state on all datasets under study. However, the stability performances of some other models are not so pronounced as that of the IAE-LSTM-KL model. For example, dramatic fluctuations of AUROC values in LSA model are observed on all datasets. On the WTBI dataset, the LSA, Deep SVDD and IAEAD models yield heavier fluctuations than the IAE-LSTM-KL model. Although CAE and VAE models can also produce trivial fluctuations in AUROC values on all three datasets, AUROC values of CAE and VAE models cannot stabilize in the level as high as that of the IAE-LSTM-KL model. This result indicates that the proposed IAE-LSTM-KL model presents better stability in the training stage than other competing models.

In order to evaluate the performance and resilience

TABLE IV: AUROC for the MVTec AD dataset. The subscripts (s) and (h) refer to the soft-boundary and hard-boundary, respectively. We highlight in bold the performance of the top-performing models.

Class	CAE	MemAE	VAE	LSA	Deep SVDD _(h)	Deep SVDD _(s)	IAEAD _(h)	IAEAD _(s)	Ours _(h)	Ours _(s)
Bottle	0.980	0.973	0.506	0.888	0.901	0.925	0.883	0.886	0.940	0.945
Cable	0.768	0.753	0.595	0.724	0.839	0.843	0.673	0.673	0.856	0.850
Capsule	0.619	0.627	0.523	0.555	0.753	0.616	0.512	0.529	0.713	0.716
Carpet	0.532	0.546	0.409	0.486	0.704	0.679	0.569	0.581	0.800	0.666
Grid	0.810	0.800	0.643	0.749	0.887	0.505	0.776	0.804	0.906	0.904
Hazelnut	0.860	0.860	0.595	0.602	0.718	0.734	0.667	0.623	0.756	0.757
Leather	0.477	0.748	0.416	0.402	0.615	0.492	0.792	0.647	0.571	0.662
Metal nut	0.569	0.541	0.272	0.570	0.877	0.853	0.323	0.489	0.735	0.761
Pill	0.759	0.759	0.441	0.703	0.808	0.806	0.643	0.643	0.768	0.758
Screw	0.482	0.707	0.522	0.038	0.137	0.093	0.328	0.285	0.963	0.869
Tile	0.582	0.541	0.708	0.678	0.740	0.738	0.758	0.701	0.723	0.796
Toothbrush	0.985	0.988	0.357	0.923	1.000	0.997	0.902	0.899	1.000	1.000
Transistor	0.801	0.771	0.603	0.741	0.876	0.847	0.720	0.763	0.889	0.900
Wood	0.914	0.910	0.922	0.924	0.757	0.850	0.969	0.938	0.927	0.959
Zipper	0.871	0.853	0.360	0.657	0.872	0.798	0.792	0.564	0.825	0.877
Avg.	0.734	0.759	0.525	0.643	0.766	0.718	0.687	0.668	0.825	0.828

of our proposed IAE-LSTM-KL model in the presence of increased abnormal samples within the dataset, we manipulate the proportion of abnormal samples and replicate the aforementioned experiments on CIFAR10 and Fashion MNIST datasets. In each dataset, the abnormal data samples are randomly chosen from the remaining nine categories. Then, the chosen abnormal data samples are added into the normal samples to form the augmented training sets. Abnormal ratios in the augmented training are set to 5%, 10%, 15%, 20%, and 25%, respectively. The impact of abnormal ratios on AUROC for all competing models in our study is presented in Fig. 5. To illustrate the statistical findings across all models, we calculate the average AUROC values over all ten classes on each dataset. Fig. 5 reveals some interesting results. Firstly, with an increase of abnormal samples in the training set, downward trends in the average AUROC values are observed for all models under study. This observation is straightforward, as a higher anomaly ratio in the training set introduces more noises into the training process, ultimately leading to degradation in the performance of anomaly detection. More importantly, our proposed IAE-LSTM-KL model consistently demonstrates higher AUROC values than other competing models, regardless of the anomaly level in the training set. This result suggests that the IAE-LSTM-KL model exhibits superior anomaly-detection capabilities across varying levels of noise in the training set when compared to other competing models.

C. Hyperparameter discussion

In this section, we shall investigate the effect of hyperparameters λ_1 and λ_2 on AUROC values. This experiment is implemented using Adam optimizer [25] and PyTorch Lightning framework [26]. For each of

CIFAR10 or Fashion MNIST dataset, λ_1 and λ_2 are adjusted separately for each class within the dataset to be normal via Optuna framework [27]. Batch sizes are set to 100 for CIFAR10 and Fashion MNIST datasets, and 128 for the WTBI dataset. The hyperparameter λ_3 in (15) and (16), which control the weight decay term, is fixed as $0.5e-6$.

Fig. 6 and Fig. 7 illustrate the impact of λ_1 and λ_2 on AUROC value for the proposed IAE-LSTM-KL model. We observe promising experimental results on Fashion MNIST and WTBI datasets. It is found that when both the two positive hyperparameters are less than 1, the IAE-LSTM-KL model yields higher AUROC values on Fashion MNIST and WTBI datasets. However, the CIFAR10 dataset does not exhibit such characteristics. This result may be attributed to the fact that the images in the CIFAR10 dataset contain three channels. Multiple channels introduce more complexities to our model and subsequently affect the trend chart of hyperparameters, which make it challenging to discern trends of anomaly-detection performance affected by λ_1 and λ_2 . On the contrary, the images on both Fashion MNIST and WTBI datasets only contain a single channel, allowing for clear trend observations for the effect of λ_1 and λ_2 on anomaly-detection performances.

D. Ablation Studies

To further investigate the role of each module in the IAE-LSTM-KL model on the performance of anomaly detection, we have also implemented ablation studies for the IAE-LSTM-KL models. Experimental results on CIFAR10, Fashion MNIST and WTBI datasets are demonstrated in Table V, Table VI and Table VII respectively. Results on MVTec AD dataset are shown in Table VIII and Table IX. These experiments aim to

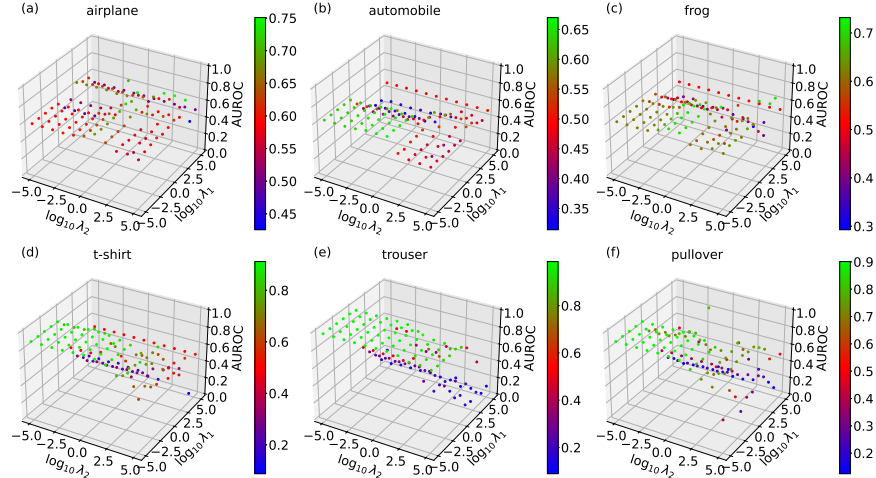


Fig. 6: Impact of hyperparameters (λ_1 and λ_2) on AUROC values on the CIFAR10 and Fashion MNIST for the IAE-LSTM-KL model. For CIFAR10, the airplane, automobile and frog classes are chosen as normal data in (a), (b) and (c) respectively. For Fashion MNIST, the t-shirt, trouser and pullover classes are chosen as normal data in (d), (e) and (f) respectively.

TABLE V: AUROC for the CIFAR10 dataset. The subscripts (s) and (h) refer to the soft-boundary and hard-boundary, respectively. We highlight in bold the performance of the top-performing models.

Class	airplane	automobile	bird	cat	deer	dog	frog	horse	ship	truck	Avg.
DSVDD-KL _(h)	0.627	0.626	0.546	0.544	0.616	0.608	0.542	0.624	0.732	0.671	0.614
DSVDD-KL _(s)	0.629	0.638	0.562	0.542	0.595	0.601	0.589	0.618	0.741	0.667	0.618
DLSVDD _(h)	0.603	0.634	0.486	0.610	0.579	0.644	0.618	0.647	0.775	0.723	0.632
DLSVDD _(s)	0.605	0.638	0.495	0.610	0.573	0.639	0.621	0.649	0.778	0.722	0.633
DLSVDD-KL _(h)	0.689	0.642	0.528	0.604	0.585	0.638	0.625	0.643	0.782	0.722	0.646
DLSVDD-KL _(s)	0.620	0.642	0.521	0.611	0.603	0.638	0.632	0.650	0.780	0.712	0.641
IAE-KL _(h)	0.764	0.659	0.607	0.649	0.711	0.680	0.729	0.658	0.817	0.766	0.704
IAE-KL _(s)	0.768	0.581	0.538	0.600	0.629	0.629	0.679	0.605	0.777	0.704	0.651
IAE-LSTM _(h)	0.667	0.680	0.504	0.633	0.626	0.636	0.719	0.645	0.793	0.760	0.666
IAE-LSTM _(s)	0.708	0.644	0.549	0.593	0.625	0.656	0.663	0.622	0.767	0.712	0.654
IAE-LSTM-KL _(h)	0.780	0.688	0.613	0.648	0.706	0.650	0.759	0.658	0.798	0.777	0.708
IAE-LSTM-KL _(s)	0.761	0.642	0.611	0.670	0.703	0.695	0.725	0.643	0.752	0.735	0.694

TABLE VI: AUROC for the Fashion MNIST dataset. The subscripts (s) and (h) refer to the soft-boundary and hard-boundary, respectively. We highlight in bold the performance of the top-performing models.

Class	t-shirt	trouser	pullover	dress	coat	sandal	shirt	sneaker	bag	ankle-boot	Avg.
DSVDD-KL _(h)	0.891	0.978	0.891	0.904	0.915	0.829	0.804	0.974	0.905	0.991	0.908
DSVDD-KL _(s)	0.887	0.978	0.890	0.902	0.916	0.889	0.804	0.971	0.911	0.991	0.914
DLSVDD _(h)	0.887	0.981	0.892	0.909	0.899	0.869	0.805	0.972	0.942	0.978	0.913
DLSVDD _(s)	0.884	0.980	0.888	0.918	0.908	0.903	0.813	0.973	0.934	0.981	0.918
DLSVDD-KL _(h)	0.884	0.982	0.895	0.912	0.903	0.873	0.809	0.971	0.948	0.981	0.916
DLSVDD-KL _(s)	0.887	0.981	0.891	0.915	0.912	0.923	0.815	0.973	0.944	0.981	0.922
IAE-KL _(h)	0.899	0.979	0.892	0.912	0.922	0.838	0.808	0.989	0.936	0.991	0.917
IAE-KL _(s)	0.906	0.971	0.868	0.906	0.913	0.841	0.809	0.984	0.921	0.994	0.911
IAE-LSTM _(h)	0.908	0.987	0.898	0.942	0.929	0.873	0.808	0.989	0.952	0.990	0.928
IAE-LSTM _(s)	0.920	0.972	0.865	0.924	0.910	0.909	0.782	0.980	0.915	0.987	0.916
IAE-LSTM-KL _(h)	0.915	0.987	0.905	0.945	0.928	0.874	0.814	0.990	0.955	0.992	0.931
IAE-LSTM-KL _(s)	0.887	0.981	0.891	0.915	0.912	0.923	0.815	0.973	0.944	0.981	0.922

discern the individual contribution and impact of each module on the overall performance of IAE-LSTM-KL

model, providing insights into the effectiveness of such enhancements in deep learning architecture. The notation

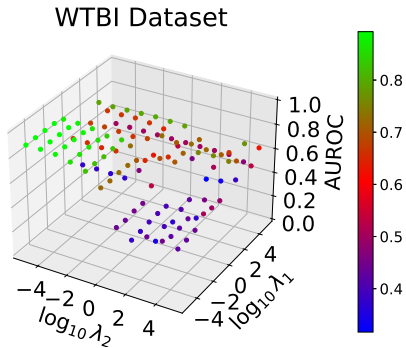


Fig. 7: Impact of hyperparameters (λ_1 and λ_2) on AUROC values on the WTBI dataset for the IAE-LSTM-KL model.

TABLE VII: AUROC for the WTBI dataset. The subscripts (s) and (h) refer to the soft-boundary and hard-boundary, respectively. We emphasize in bold the performance of the best models.

Models	AUROC
DSVDD-KL _(h)	0.802
DSVDD-KL _(s)	0.810
DLSVDD _(h)	0.899
DLSVDD _(s)	0.945
DLSVDD-KL _(h)	0.902
DLSVDD-KL _(s)	0.944
IAE-KL _(h)	0.801
IAE-KL _(s)	0.894
IAE-LSTM _(h)	0.892
IAE-LSTM _(s)	0.952
IAE-LSTM-KL _(h)	0.908
IAE-LSTM-KL _(s)	0.963

of each model under comparison with the IAE-LSTM-KL model is described as following:

- DSVDD-KL: Compared with the IAE-LSTM-KL model, this model does not include the LSTM module. In addition, the decoder part in CAE is also not included in this model. Therefore, the objective function of this model only contains SVDD loss and KL-divergence loss.
- DLSVDD: Compared with the IAE-LSTM-KL model, this model does not include the decoder part in CAE. In addition, due to the absence of KL divergence, the latent feature vector after the encoder is not forced to follow Gaussian distribution. The objective function of this model only contains the SVDD loss.
- DLSVDD-KL: Compared with the IAE-LSTM-KL model, this model only does not include the decoder part in CAE. In other words, the DLSVDD-KL model is formed by restricting the latent feature vector after LSTM module in DLSVDD model

following the Gaussian distribution. The objective function of this model contains the SVDD loss and KL-divergence loss.

- IAE-KL: The only difference of this model from the IAE-LSTM-KL model is that this model does not include the LSTM module.
- IAE-LSTM: The only difference of this model from the IAE-LSTM-KL model is that this model does not incorporate KL divergence to force the latent feature vector following the Gaussian distribution.

Experiments have been implemented to study the importance of each module by leveraging different combinations and permutations of the CAE module, the SVDD module, the LSTM module and the operation of KL divergence. Comparing results among the IAE-LSTM-KL model and its competing counterparts on CIFAR10, Fashion MNIST, WTBI and MVTec AD datasets are demonstrated in Table V, Table VI, Table VII, Table VIII and Table IX respectively, we find that in most cases, the IAE-LSTM-KL model yields the highest AUROC values than other models with some module (or modules) removed from the IAE-LSTM-KL model. The results indicate that the combination of SVDD module, CAE module, LSTM module and KL divergence can indeed enhance the performance of anomaly detection.

V. CONCLUSION

In this paper, we propose a novel anomaly-detection model, called Improved AutoEncoder with LSTM module and KL divergence (IAE-LSTM-KL) model, to further enhance the performance of anomaly detection. This model adds an LSTM module between the encoder and the decoder to mitigate the over-generalization of traditional convolutional autoencoder model in reconstructing abnormal input. In addition, an SVDD module is connected to the output of LSTM module to jointly train the whole IAE-LSTM-KL model. The Kullback-Leibler (KL) divergence regulating the input data of SVDD module following Gaussian distribution is used to mitigate the chance of hypersphere collapse in SVDD module. That is to say, the proposed IAE-LSTM-KL model has the effect of reducing false negative rate as compared to the traditional convolutional autoencoder model. In the meanwhile, local structure of input can be preserved by incorporating SVDD model with the use of KL divergence to avoid hypersphere collapse when training SVDD module.

Extensive experiments have been carried out to compare the performance of the proposed IAE-LSTM-KL model with a few other state-of-art models on both synthetic and real-world datasets. Results show that the proposed IAE-LSTM-KL model yields higher detection precision for anomalies. Besides, we have also found

TABLE VIII: AUROC for the MVTec AD dataset. The subscripts (s) and (h) refer to the soft-boundary and hard-boundary, respectively. We highlight in bold the performance of the top-performing models.

Class	DSVDD-KL _(h)	DSVDD-KL _(s)	DLSVDD _(h)	DLSVDD _(s)	DLSVDD-KL _(h)	DLSVDD-KL _(s)
Bottle	0.906	0.881	0.945	0.931	0.932	0.929
Cable	0.839	0.840	0.847	0.848	0.853	0.846
Capsule	0.753	0.709	0.684	0.715	0.730	0.711
Carpet	0.688	0.617	0.678	0.628	0.659	0.625
Grid	0.907	0.736	0.815	0.851	0.780	0.828
Hazelnut	0.706	0.738	0.705	0.768	0.716	0.757
Leather	0.564	0.551	0.577	0.558	0.518	0.569
Metal nut	0.876	0.737	0.774	0.742	0.746	0.741
Pill	0.810	0.724	0.744	0.728	0.761	0.728
Screw	0.091	0.194	0.398	0.270	0.649	0.800
Tile	0.745	0.691	0.560	0.754	0.725	0.748
Toothbrush	1.000	0.988	0.985	0.997	0.997	0.997
Transistor	0.874	0.880	0.891	0.889	0.881	0.888
Wood	0.767	0.754	0.660	0.775	0.790	0.768
Zipper	0.870	0.862	0.739	0.867	0.828	0.867
Avg.	0.760	0.727	0.733	0.755	0.771	0.787

TABLE IX: AUROC for the MVTec AD dataset. The subscripts (s) and (h) refer to the soft-boundary and hard-boundary, respectively. We highlight in bold the performance of the top-performing models.

Class	IAE-KL _(h)	IAE-KL _(s)	IAE-LSTM _(h)	IAE-LSTM _(s)	IAE-LSTM-KL _(h)	IAE-LSTM-KL _(s)
Bottle	0.903	0.921	0.940	0.944	0.940	0.945
Cable	0.838	0.844	0.856	0.849	0.856	0.850
Capsule	0.750	0.664	0.708	0.720	0.713	0.716
Carpet	0.743	0.701	0.663	0.630	0.800	0.666
Grid	0.897	0.370	0.805	0.847	0.906	0.904
Hazelnut	0.672	0.658	0.733	0.756	0.756	0.757
Leather	0.581	0.558	0.535	0.583	0.571	0.662
Metal nut	0.877	0.862	0.730	0.743	0.735	0.761
Pill	0.811	0.816	0.769	0.756	0.768	0.758
Screw	0.180	0.108	0.466	0.249	0.963	0.869
Tile	0.740	0.712	0.718	0.780	0.723	0.796
Toothbrush	1.000	0.991	1.000	0.997	1.000	1.000
Transistor	0.876	0.868	0.889	0.895	0.889	0.900
Wood	0.759	0.828	0.923	0.953	0.927	0.959
Zipper	0.873	0.793	0.824	0.877	0.825	0.877
Avg.	0.767	0.713	0.771	0.772	0.825	0.828

that even though when the training set is contaminated with outliers, the detection rate for anomalies of the IAE-LSTM-KL model can still stabilize in the higher level than other competing models. In a word, both the effectiveness and robustness of anomaly-detection can be enhanced by using the IAE-LSTM-KL model.

REFERENCES

- [1] N. Shone, T. N. Ngoc, V. D. Phai, and Q. Shi, “A deep learning approach to network intrusion detection,” *IEEE Trans. Emerg. Topic Comput. Intell.*, vol. 2, no. 1, pp. 41–50, Feb. 2018.
- [2] D. Huang, D. Mu, L. Yang, and X. Cai, “Codetect: Financial fraud detection with anomaly feature detection,” *IEEE Access*, vol. 6, pp. 19 161–19 174, 2018.
- [3] X. Zhang, S. Li, X. Li, P. Huang, J. Shan, and T. Chen, “Destseg: Segmentation guided denoising student-teacher for anomaly detection,” in *Proc. IEEE/CVF Conf. Comput. Vis. Pattern Recognit. (CVPR)*, Jun. 2023, pp. 3914–3923.
- [4] R. Zhang, P. Isola, and A. A. Efros, “Split-brain autoencoders: Unsupervised learning by cross-channel prediction,” in *Proc. IEEE Conf. Comput. Vis. Pattern Recognit.*, Jul. 2017, pp. 1058–1067.
- [5] I. Golan and R. El-Yaniv, “Deep anomaly detection using geometric transformations,” in *32nd Conf. on Neur. Inf. Proc. Syst.*, 2018, pp. 9781–9791.
- [6] J. Masci, U. Meier, D. Cireřan, and J. Schmidhuber, “Stacked convolutional auto-encoders for hierarchical feature extraction,” in *Artificial Neural Networks and Machine Learning—ICANN*. Springer, June 2011, pp. 52–59.

- [7] D. P. Kingma and M. Welling, “Auto-encoding variational bayes,” *arXiv:1312.6114*, 2013.
- [8] D. Gong, L. Liu, V. Le, B. Saha, M. R. Mansour, S. Venkatesh, and A. v. d. Hengel, “Memorizing normality to detect anomaly: Memory-augmented deep autoencoder for unsupervised anomaly detection,” in *Proc. Int. Conf. Comput. Vis.*, Oct. 2019, pp. 1705–1714.
- [9] S. Tuli, G. Casale, and N. R. Jennings, “TranAD: Deep Transformer Networks for Anomaly Detection in Multivariate Time Series Data,” *Proc. VLDB Endowment*, vol. 15, no. 6, pp. 1201–1214, Feb. 2022.
- [10] D. M. Tax and R. P. Duin, “Support vector data description,” *Mach. Learn.*, vol. 54, no. 1, pp. 45–66, 2004.
- [11] L. Ruff, R. Vandermeulen, N. Goernitz, L. Deecke, S. A. Siddiqui, A. Binder, E. Müller, and M. Kloft, “Deep one-class classification,” in *Proc. Int. Conf. Mach. Learn.*, vol. 80, 2018, pp. 4393–4402.
- [12] F. V. Massoli, F. Falchi, A. Kantarci, Ş. Akti, H. K. Ekenel, and G. Amato, “MOCCA: Multilayer one-class classification for anomaly detection,” *IEEE Trans. Neural Netw. Learn. Syst.*, vol. 33, no. 6, pp. 2313–2323, 2021.
- [13] J. Yi and S. Yoon, “Patch SVDD: Patch-level SVDD for anomaly detection and segmentation,” in *Proc. Asian Conf. Comput. Vis.*, 2020, pp. 375–390.
- [14] Z. Cheng, S. Wang, P. Zhang, S. Wang, X. Liu, and E. Zhu, “Improved autoencoder for unsupervised anomaly detection,” *Int. J. Intell. Syst.*, vol. 36, no. 12, pp. 7103–7125, Dec. 2021.
- [15] S. Hochreiter and J. Schmidhuber, “Long short-term memory,” *Neural Comput.*, vol. 9, no. 8, pp. 1735–1780, 1997.
- [16] A. Krizhevsky and G. Hinton, “Learning multiple layers of features from tiny images,” 2009. [Online]. Available: <https://www.cs.toronto.edu/~kriz/learning-features-2009-TR.pdf>
- [17] H. Xiao, K. Rasul, and R. Vollgraf, “Fashion-mnist: a novel image dataset for benchmarking machine learning algorithms,” *arXiv:1708.07747*, 2017.
- [18] P. Bergmann, M. Fauser, D. Sattlegger, and C. Steger, “Mvtec ad—a comprehensive real-world dataset for unsupervised anomaly detection,” in *Proc. IEEE Conf. Comput. Vis. Pattern Recognit.*, Jun. 2019, pp. 9592–9600.
- [19] W. Liu, W. Luo, D. Lian, and S. Gao, “Future frame prediction for anomaly detection—a new baseline,” in *Proc. IEEE Conf. Comput. Vis. Pattern Recognit.*, 2018, pp. 6536–6545.
- [20] Z. Liu, Y. Nie, C. Long, Q. Zhang, and G. Li, “A hybrid video anomaly detection framework via memory-augmented flow reconstruction and flow-guided frame prediction,” in *Proc. IEEE/CVF Int. Conf. Comput. Vis. (ICCV)*, 2021, pp. 13 588–13 597.
- [21] J. Wyatt, A. Leach, S. M. Schmon, and C. G. Willcocks, “Anoddpn: Anomaly detection with denoising diffusion probabilistic models using simplex noise,” in *Proc. IEEE/CVF Conf. Comput. Vis. Pattern Recognit. (CVPR)*, 2022, pp. 650–656.
- [22] D. Abati, A. Porrello, S. Calderara, and R. Cucchiara, “Latent space autoregression for novelty detection,” in *Proc. IEEE/CVF Conf. Comput. Vis. Pattern Recognit. (CVPR)*, 2019, pp. 481–490.
- [23] S. Ioffe and C. Szegedy, “Batch normalization: Accelerating deep network training by reducing internal covariate shift,” in *Proc. Int. Conf. Mach. Learn.*, 2015, pp. 448–456.
- [24] A. L. Maas, A. Y. Hannun, and A. Y. Ng, “Rectifier nonlinearities improve neural network acoustic models,” in *Proc. Int. Conf. Mach. Learn.*, vol. 30, no. 1. Atlanta, GA, 2013, pp. 1–6.
- [25] D. P. Kingma and J. Ba, “Adam: A method for stochastic optimization,” *arXiv:1412.6980*, 2014.
- [26] W. Falcon and The PyTorch Lightning team, “PyTorch Lightning,” Mar. 2019. [Online]. Available: <https://github.com/Lightning-AI/lightning>
- [27] T. Akiba, S. Sano, T. Yanase, T. Ohta, and M. Koyama, “Optuna: A next-generation hyperparameter optimization framework,” in *Proc. 25th ACM SIGKDD Int. Conf. Knowl. Discovery Data Mining*, Jul. 2019, pp. 2623–2631.



Wei Huang received the M.S. degree in Circuits and Systems from University of Electronic Science and Technology of China (UESTC), Chengdu, China, in 2007, and the Ph.D. degree in Electronic Engineering from City University of Hong Kong, China, in 2011. He is currently an associate Professor with the College of Computer Science and Technology, Zhejiang University of Technology (ZJUT), Hangzhou, China. His current research interests include machine learning, data mining and machine intelligence.



Bingyang Zhang received the Bachelor's degree in Data Science and Big Data technology from Zhejiang University of Technology in 2022, and is currently pursuing a Master's degree in Computer Science and Technology at Zhejiang University of Technology. His main research interests include machine learning, data mining and anomaly detection.



Kaituo Zhang is an undergraduate student currently pursuing studies at Zhejiang University of Technology. His current research interests include machine learning, data mining and anomaly detection.



Hua Gao received the B.S. degree in information and computing science from Shandong University, Weihai, China, in 2005. He received the M.S. and Ph.D degrees from Nanjing University of Technology, Nanjing, China, in 2007 and 2013, respectively. He is currently a lecturer with the School of Computer Science and Technology, Zhejiang University of Technology. He has authored or coauthored more than 10 research papers in machine learning, information fusion, and image understanding. His current research interests include pattern recognition, machine learning, and intelligent systems.



Rongchun Wan received the B.S. degree in automation from Hangzhou Institute of Electronic Technology in 2003. He works as a Technical Director in Zhejiang HOUDAR Intelligent Technology Co., Ltd. His current research interests include development & design of intelligent equipment, and collection and analysis of production data.